photonics

MDPI

Communication

Demonstration of Power-over-Fiber with Watts of Output Power Capabilities over Kilometers or at Cryogenic Temperatures

Simon Fafard * and Denis Masson

Broadcom (Canada), Industrial Fiber Product Division (IFPD), Ottawa, ON K1A 0R6, Canada; denis.masson@broadcom.com

* Correspondence: simon.fafard@broadcom.com

Abstract: We demonstrate the use of laser diodes and multijunction photovoltaic power converters to efficiently deliver watts of electrical power for long-distance or cryogenic applications. Transmission through single-mode and multi-mode fibers at the wavelengths of 808 nm and 1470/1550 nm are studied. An electrical output power of ~0.1 W is obtained after a 5 km transmission through a standard single-mode SMF28 fiber fed with 0.25 W of optical power. An electrical output power of ~1 W is demonstrated after a 5 km transmission with a standard OM1 multi-mode fiber fed with ~2.5 W. Photovoltaic conversion efficiencies reaching Eff ~49% are obtained with an output voltage of ~5 V using commercial multijunction laser power converters. For low-temperature applications, an ultra-sensitive silicon photomultiplier (SiPM) is used to detect the residual light leaked from fibers as the temperature is decreased. Our study demonstrates that specific fiber types enable low-loss transmission compatible with cryogenic requirements and without light leakage triggering of the SiPM. A cryogenic power-over-fiber system at ~1470 nm is demonstrated with ~2 W of electrical power converted over a 10 m distance having a conversion efficiency of Eff > 65% at 77 K.

Keywords: power-over-fiber; optical power converters; laser power converters; photovoltaic multijunctions; galvanic isolation; InGaAs; InP; single-mode fiber; multi-mode fiber; cryogenic

Citation: Fafard, S.; Masson, D. Demonstration of Power-over-Fiber with Watts of Output Power Capabilities over Kilometers or at Cryogenic Temperatures. *Photonics* **2024**, *11*, 596. https://doi.org/10.3390/photonics11070596

Received: 4 June 2024
Revised: 24 June 2024
Accepted: 25 June 2024
Published: 26 June 2024

1. Introduction

The prospects and the applications of optical power delivery based on power-over-fiber (PoF, referring to fully optical energy transfer) or on optical wireless power transmission (OWPT) systems have greatly evolved over the years [1–23]. PoF technologies continue to offer many attractive features and to stimulate new developments at various wavelengths. For example, increasing the transmission distance and the optical power transmitted are two developments of prime interest. For other applications, cryogenic temperature capabilities with minimal parasitic light leakage can be the main objectives, while still maintaining full galvanic isolation. This is the case for liquid argon or liquid xenon high-voltage time-projection chambers for fundamental neutrino detection and dark matter studies, or for cosmic muon research [24–30]. For applications requiring kilometers of optical power transmission, it is advantageous to develop PoF systems based on economically viable solutions, for example, using standard single-mode fiber (SMF) or multi-mode (MM) fiber cables.

The optical power delivery limits of standard SMF have been previously studied to understand the impact of transmission losses, the nonlinear effect of stimulated Raman scattering (SRS), and the nonlinear effect caused by Brillouin scattering [1,3]. These earlier studies indicated that relatively broadband light sources at wavelengths around 1550 nm can be advantageous to successfully suppress Brillouin scattering losses and to minimize the transmission losses.

Concurrently, recent progress with vertical multijunction laser power converters (LPCs), also called optical power converters (OPCs), has empowered a new class of com-

mercial high-efficiency ~5 V photovoltaic devices. They have been productized for the 1450–1550 nm spectral range and also for cryogenic applications at ~1470 nm or ~808 nm [31–34]. Furthermore, the unrelenting developments in the field of photovoltaic devices further promise additional LPC device opportunities [35–43].

The goal of this study is therefore to exemplify the use of laser diodes to deliver watts of electrical power for long-distance or cryogenic applications based on such new multijunction LPCs. We verified the transmission through commercial single-mode and multi-mode fibers at wavelengths of 808 nm and 1470/1550 nm. At 1550 nm, our study demonstrated an electrical output power of up to ~0.1 W (limited by the laser diode output power) after a 5 km transmission distance with a standard single-mode SMF28 fiber [44]. At a wavelength of ~1470 nm, an electrical output power of ~1 W after a 5 km transmission distance was demonstrated with a standard OM1 multi-mode fiber [44]. Remote photovoltaic conversion efficiencies reaching Eff ~49% were demonstrated with an output voltage of ~5 V using these multijunction laser power converters.

For low-temperature applications, an ultra-sensitive silicon photomultiplier (SiPM) was used to detect the residual light leaked from fibers as the temperature decreased. We demonstrated that specific fiber types enable low-loss transmission compatible with cryogenic requirements and without any residual light leakage that could otherwise trigger the SiPM. A cryogenic power-over-fiber system at ~1470 nm was demonstrated with ~2 W of electrical power converted over a 10 m distance, having a conversion efficiency of Eff ~65.7% at 77 K.

2. Materials and Methods

The LPC structure was based on the vertical epitaxial heterostructure architecture (VEHSA) design [22,31]. The 1470/1550 nm LPCs used InGaAs absorbing layers lattice-matched to InP: PT10-InGaAs/InP. Fabricated chips with an area of ~0.032 cm^2 were packaged in Broadcom's *Regular Power* format, with an FC optical connector [32]. The 808 nm LPCs used GaAs absorbing layers on GaAs: PT5-GaAs [33]. In all cases, the Beer–Lambert law was used to determine the thicknesses of the individual subcells, with the target of having each subcell absorbing an equivalent fraction of the incident light for the wavelengths and temperatures of interest. To realize the required photocurrent-matching condition, the subcells had increasing thicknesses from the top subcell (thinnest) toward the bottom subcell (thickest) [34]. The methodology for applying the Beer–Lambert approach has been described previously [31], and no corrections were implemented in the present study for photon coupling and recycling, or other second-order effects or optimizations.

The subcells were interconnected with optically transparent tunnel junctions; each individual subcell comprised an n-type emitter and a p-type base (i.e., n on p configuration). The tunnel junctions were made to be transparent to the input beam, utilizing AlGaInAs alloys that were lattice-matched to InP or AlGaAs for the GaAs-based LPCs. The epitaxial layers were grown using commercial production Aixtron Metal–Organic Chemical Vapor Deposition (MOCVD) reactors.

The epitaxial wafers were fabricated with a standard blanket back-metallization, front ohmic contacts, and antireflection coatings (ARCs) constructed from layers of Al_2O_3 and TiO_2. An ARC typically reduces the reflectivity (R) of the incident beam to R < 4% for the spectral range of interest. All devices were tested using dark I–V measurements. The wafers had a high level of chip uniformity, as assessed from such dark I–V tests. The device performance results have been reported in detail previously [31–34]. Similarly, here, for the performance measurements, the I–V characteristics were acquired using a Keithley 2601B source-meter in a four-wire probing mode. Quick I–V scans were used, with a duration of about 1 s, to avoid significant chip heating. After the transmission through the fiber, FC connectors were used to connect the fiber output end to the LPC device.

Three main different laser types were used in this study. BWT laser diodes [45] were used as multi-mode sources: 7 W~1470 nm sources with a 105 µm core were used for the MM experiments at 20 °C; similar lasers were used as 3 W~1550 nm sources; 8 W~808 nm

sources with a 400 μm core were used for the MM experiments at 77 K; and finally, a 0.25 W SemiNex laser diode was used as a high-power single-mode 1550 nm source with a 10 nm spectral width [46].

3. Results

Figure 1 shows the measured dependence of the transmission losses on the length of the optical fiber for standard single-mode and multi-mode fibers. The single-mode fiber was a Corning SMF28-Ultra with a core diameter of 8.2 μm, cladding of 125 μm, and NA ~0.14. It was fed from a pigtailed single-mode 1550 nm laser diode. The multi-mode fiber was a standard graded-index Corning InfiniCor OM1 fiber with a core diameter of 62.5 μm, cladding of 125 μm, and NA ~0.275. It was fed from a pigtailed multi-mode 1470 nm laser diode having a 105 μm core and an NA ~0.22. A lens-coupler was used to minimize the coupling losses between the multi-mode laser and the OM1 fiber (OzOptics' part #AA-300-33-1550-M-SP1) [47].

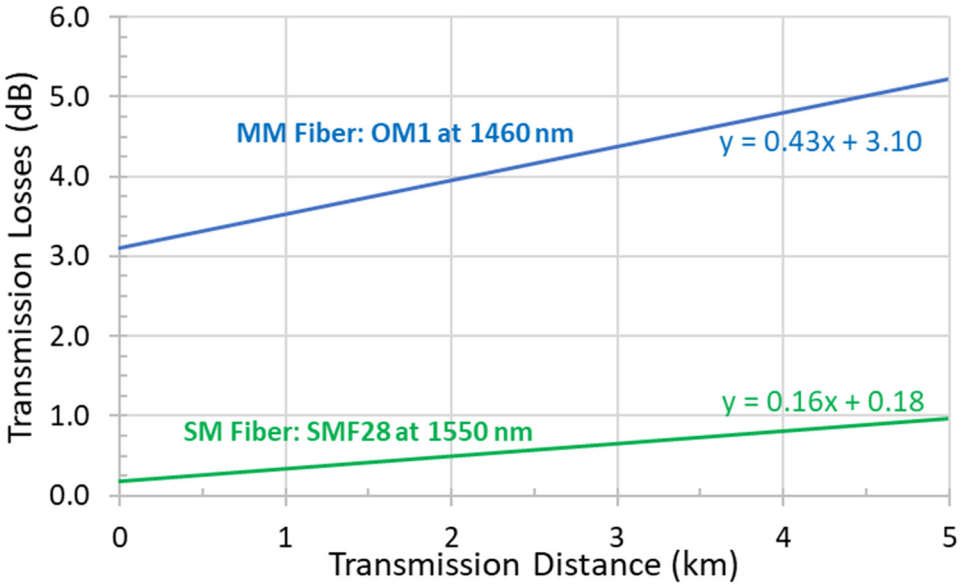

Figure 1. Transmission losses' dependence on the optical fiber length measured for standard single-mode (green curve) and multi-mode fibers (blue curve). The slopes give the dB/km loss parameters, while the intercepts represent the coupling losses from the lasers/patchcords/connectors used. The single-mode fiber is a Corning SMF28-Ultra with a core diameter of 8.2 μm, cladding of 125 μm, and NA ~0.14, which is fed from a pigtailed single-mode 1550 nm laser diode. The multi-mode fiber is a standard graded-index Corning InfiniCor OM1 fiber with a core diameter of 62.5 μm, cladding of 125 μm, and NA ~0.275 coupled from a pigtailed multi-mode 1470 nm laser diode having a 105 μm core and an NA ~0.22. A lens-coupler was used to minimize the coupling losses between the multi-mode laser and the OM1 fiber (OzOptics' part #AA-300-33-1550-M-SP1) [44–48].

For the SMF at 1550 nm, a loss of 0.16 dB/km was obtained with a coupling loss of 0.18 dB. The observed low losses are consistent with the expected values for the minimal fiber loss window near 1550 nm. The single-mode laser had a nominal spectral width of 10 nm to minimize the nonlinear transmission losses, and it had a maximum output power of 250 mW. The maximum available single-mode 1550 nm optical power was therefore ~225 mW and ~200 mW after 1 km and 5 km of transmission, respectively, as shown in Figure 2.

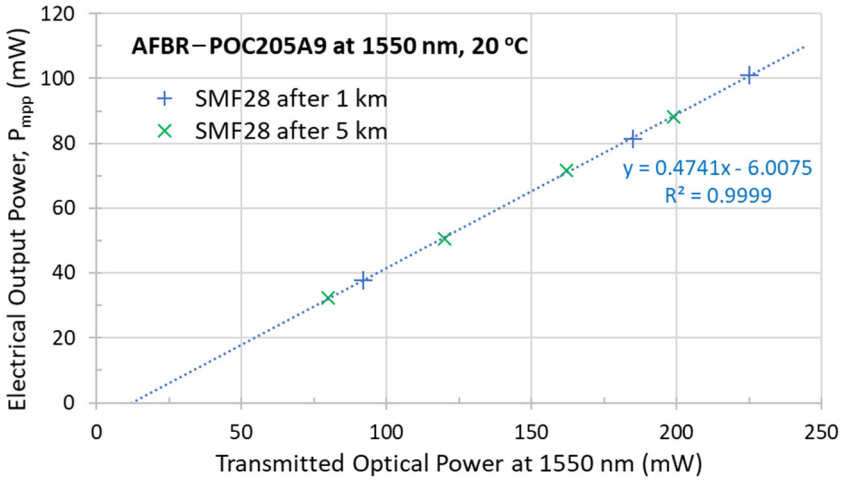

Figure 2. Measured electrical output from Broadcom's AFBR-POC205A9 multijunction PT10-InGaAs/InP laser power converter for single-mode transmission distances of 1 km (blue crosses) and 5 km (green X) with different optical input powers at 1550 nm. The transmitted optical power on the horizontal axis refers to the output power exiting the output end of the fiber.

Figure 2 shows the measured electrical output obtained with Broadcom's AFBR-POC205A9 multijunction PT10-InGaAs/InP laser power converter. It was obtained for single-mode transmission distances of 1 km (blue crosses) and 5 km (green X) with different optical input powers at 1550 nm. As can be seen from the linear regression of Figure 2, the conversion efficiency of the AFBR-POC205A9 device was about Eff = 47% for both cases, after 1 km or 5 km of optical power transmission. Consequently, it demonstrated a single-mode PoF system at 1550 nm with an electrical output power of ~0.1 W after 1 km and ~90 mW after 5 km, limited here by the relatively low-power single-mode laser used.

For PoF applications requiring more power, Figure 3 shows the case of a multi-mode fiber power link. Figure 3 also reproduces the single-mode data of Figure 2 for comparison purposes. The measured electrical output from Broadcom's [49] AFBR-POC205A8 multi-junction PT10-InGaAs/InP laser power converter is obtained for transmission distances of 1 km (purple circles at 1550 nm) and 5 km (green circles at 1470 nm). The results are measured at 20 °C for different multi-mode optical input powers. The multi-mode transmission losses at ~1470 nm were obtained, as shown in Figure 1, at 0.43 dB/km with an initial coupling loss of 3.1 dB. The coupling loss originated from the transmission from the 1470 nm laser diode with a 105 μm core fiber and an NA ~0.22 going into the OM1 fiber with a 62.5 μm core fiber and an NA ~0.275 through the lens-coupler, which was used to minimize the coupling losses [48].

The transmission loss in the multi-mode fiber was somewhat larger than that obtained with the single-mode fiber. This could be in part because the wavelength of ~1470 nm was slightly away from the minimum fiber loss window, and also because the multi-mode transmission could have had slightly higher losses. Nevertheless, because the maximum output power available from the multi-mode ~1470 nm was much higher at ~7 W, it yielded a maximum transmitted power of 2 W for the case of a multi-mode link with the 1470 nm laser. As shown in Figure 3, the resulting PoF system transmitted up to almost 1 W of available electrical power over 5 km with an LPC conversion efficiency of Eff ~49%. The slightly higher conversion efficiency observed in this case is attributable to the higher performance of the AFBR-POC205A8 at that wavelength. For comparison, Figure 3 also shows the case of 1 km multi-mode transmission at 1550 nm, which yielded a conversion efficiency of Eff ~45.5% with a maximum electrical power of almost 600 mW. The maximum electrical power for the case of multi-mode 1550 nm was lower than that at 1470 nm because the maximum output power of the 1550 nm laser diode was limited to 3 W from that laser diode.

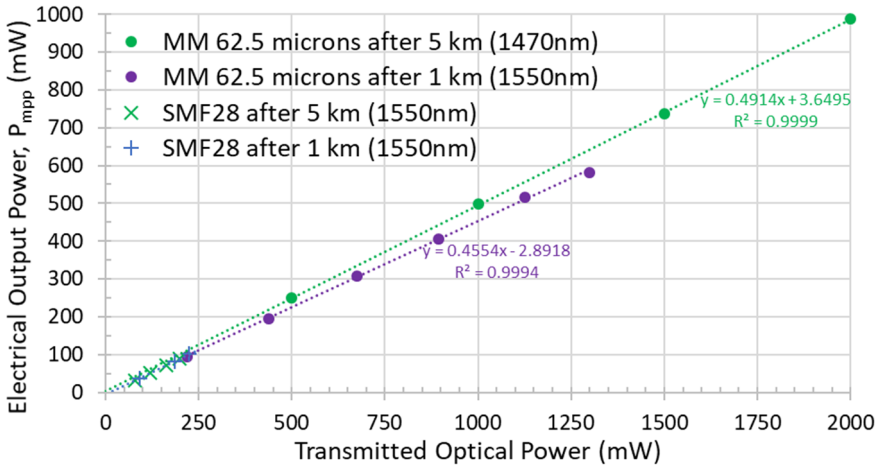

Figure 3. Measured electrical output from Broadcom's AFBR-POC205A8 multijunction PT10-InGaAs/InP laser power converter for multi-mode transmission distances of 1 km (purple circles at 1550 nm) and 5 km (green circles at 1470 nm) for different optical input powers. The single-mode data of Figure 2 are also included for comparison.

For low-temperature applications, we examined the attributes of the cryogenic LPCs at 808 nm [33] and 1470 nm [34]. The top picture in Figure 4 shows a pigtailed multi-mode 808 nm laser diode in operation at 20 °C. It clearly reveals some faint light leakage and also some slightly brighter spots along the fiber length. A similar level of light leakage is observed with other lasers. For example, the bottom pictures in Figure 4 show another similar 808 nm laser diode in operation. The bottom left picture in Figure 4 was taken with room illumination to obtain a better view of the laser pigtail furcation. The corresponding infrared smart-phone view is shown in the bottom right of Figure 4, which is highlighting the laser light leakage. For the bottom pictures in Figure 4, the pigtail was purposely set up with a 30 mm diameter loop. The laser operated with an output of ~0.8 W in this example. We clearly observed that the loop was inducing additional light leakage, even though the bending radius of the loop was not very pronounced. For a loop diameter of ~30 mm, we measured that the light leakage losses from the loop were about 5% of the output power. Furthermore, the optical power losses from the loop were fully reversible when the loop diameter was relaxed to a diameter greater than about 70 mm. Small random spots of light leakage still remained along the fiber length for all cases.

Such light leakage can certainly be problematic in cryogenic PoF systems that further require the employment of highly light-sensitive SiPM photodetectors. We therefore explore better options for avoiding such potential light-leakage issues. Furthermore, our measurements reveal that light leakage often becomes worse as the temperature is decreased, depending on the type of fiber used in the PoF system.

For example, Figure 5 shows the −40 V current of a high-sensitivity silicon photomultiplier (Broadcom's AFBR-S4xx SiPM) as a function of the ambient temperature for different fiber configurations. The SiPM and the various fibers were enclosed within a light-tight oven in a dark room. The oven was temperature-regulated and the SiPM was used to evaluate, with the highest possible sensitivity, the residual light emanating from various multi-mode optical fiber configurations. The fibers have been studied for ambient temperatures between −50 °C and 85 °C. The "common fibers" (blue and purple curves) are step-index optical fibers with a 400 µm core. They are commonly used for commercial high-power laser diodes. The laser fiber is protected with a furcation tubing jacket, as seen, for example, in the picture in Figure 4. The 808 nm result indicates that the amount of light leaked from such a common fiber configuration increases as the ambient temperature is decreased. The SiPM current for the blue curve in Figure 5 was high for the entire range and further increased by a factor of 1.7× between 20 °C and −50 °C. Fiber light leakage at lower temperatures has previously been observed and associated with compression

effects on the light-guiding glass medium of the optical fiber. The compression effects were expected to be caused by the jacket (the furcation tubing). Differences in the expansion coefficients of the dissimilar materials were expected to create micro-bends and additional light escape paths in the fiber [30].

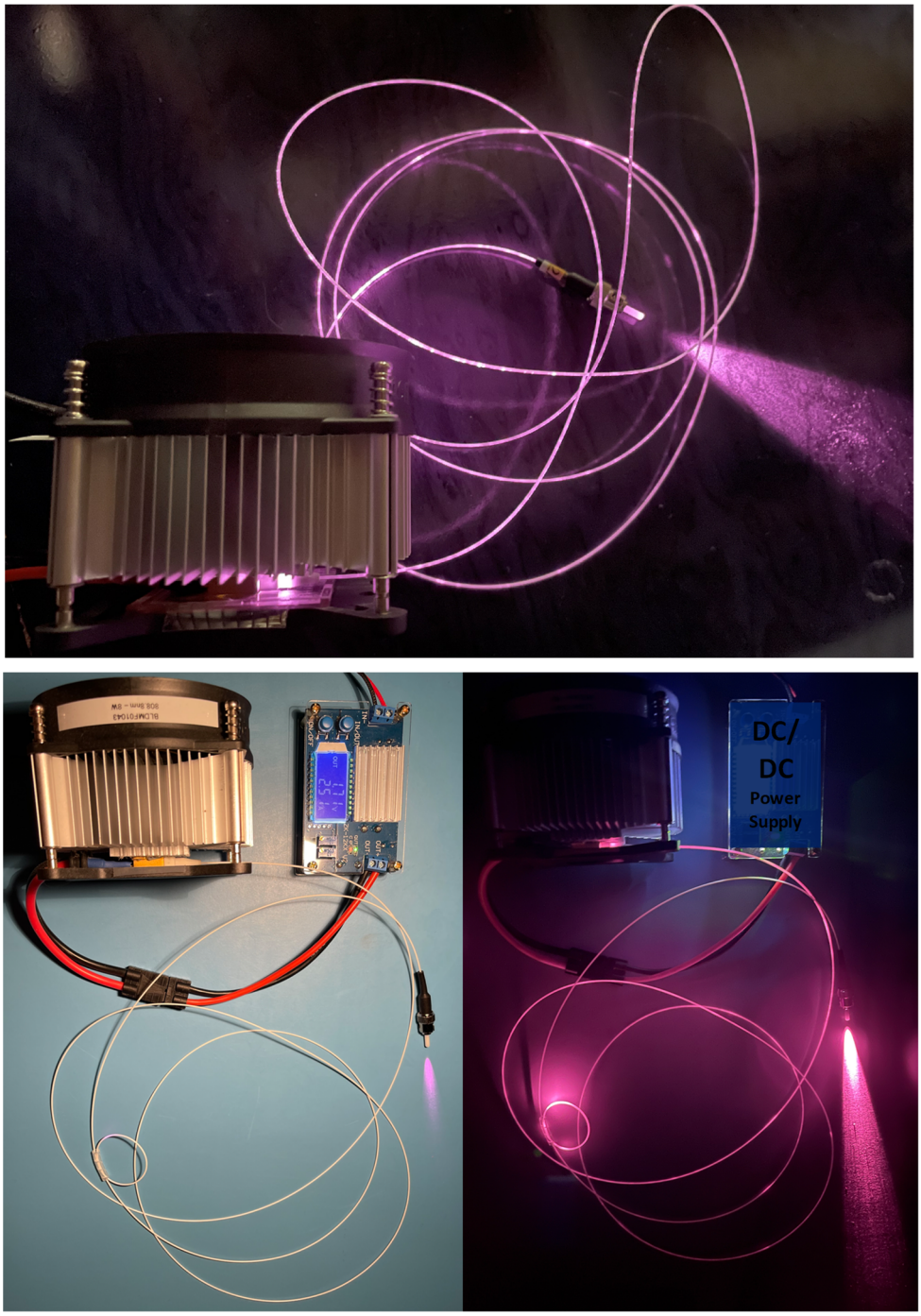

Figure 4. Picture of pigtailed multi-mode 808 nm laser diode in operation at 20 °C, revealing faint light leakage and some slightly brighter spots along the fiber length (**top**). The picture was taken from a smart-phone camera, which responded to the 808 nm light. Bottom: Another similar 808 nm laser diode in operation (powered with a DC/DC power supply) with room illumination to better view the laser pigtail (**bottom left**); and corresponding infrared smart-phone view, which highlights the laser light leakage (**bottom right**). The pigtail at the bottom was set up with a 30 mm diameter loop, which induced additional light leakage.

Even more importantly, when compared to the SiPM current in the dark (black curve: "No light"), the presence of the 808 nm transmitting fiber increased the SiPM current by several orders of magnitude. The light leakage detected by the sensitive SiPM from the 808 nm fiber was also consistent with the optical picture seen in Figure 4 and with some transmission losses observed separately (discussed further below). It should be noted that the decrease in the SiPM current with temperature for the "No light" curve is typical for a semiconductor photodetector. Furthermore, for an SiPM, the breakdown voltage is known to decrease with temperature; therefore, for a fixed voltage of −40 V, the effective overvoltage slightly increases as the temperature is decreased. This means the gain of the SiPM can be somewhat different for various temperatures, and therefore, the measured light leakage signals cannot simply be quantified directly.

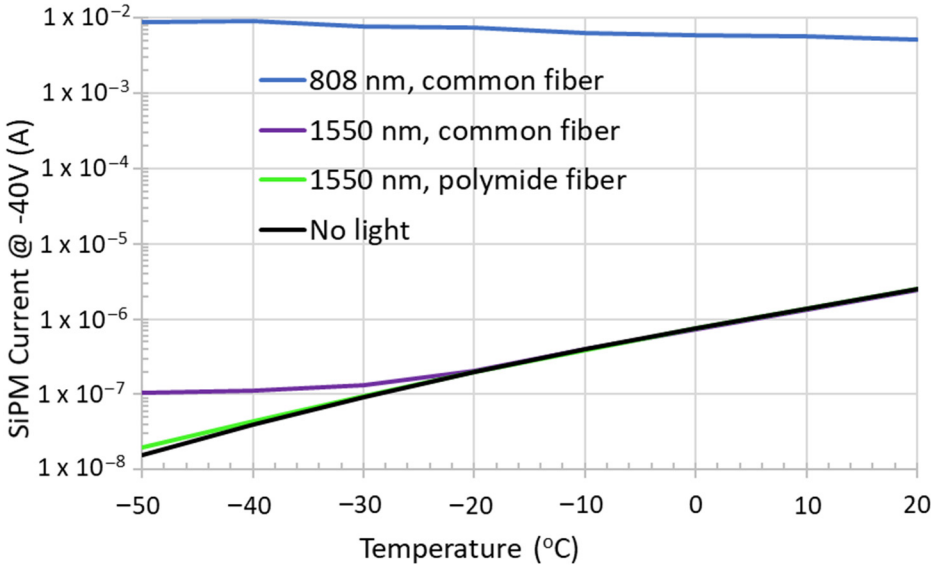

Figure 5. The −40 V dark-current of a silicon photomultiplier (Broadcom's AFBR-S4xx SiPM) was used to evaluate, with the highest possible sensitivity, the residual light emanating from various multi-mode optical fiber configurations as a function of the ambient temperature. The "common fibers" (blue and purple curves) are step-index fiber types with a 400 µm core and protected with a furcation tubing jacket, as shown in Figure 4. The "polyimide fiber" (green curve) is a bare polyimide fiber (no tubing jacket) from Thorlabs' FG400LEP multi-mode fiber with a 400 µm core and an NA ~0.22. Compared to the SiPM current in the dark (black curve: "No light"), obtained in complete darkness, the polyimide fiber exhibited no measurable light leakage over the temperature range studied.

Adopting the 1450–1550 nm wavelength range is a strategic alternative for avoiding light leakage, which can affect the SiPM current. This strategy is expected to be effective in reducing some possible interference with the SiPM's detection sensitivity. This long-wavelength spectral range is well below the silicon's bandgap and, consequently, the SiPM's response to those photons is very weak or absent. The purple curve of Figure 5 shows the results obtained for a comparable common fiber configuration for a laser operating at a wavelength of ~1550 nm. As expected, when compared to the SiPM current in the dark (black curve: "No light"), the presence of the 1550 nm transmitting fiber did not increase the SiPM current for temperatures higher than −20 °C. However, for the lower temperatures, the light leakage from the fiber at 1550 nm still affected the SiPM current, increasing the SiPM current by a factor of ~5x at −50 °C. We separately verified that the SiPM indeed appeared to have a weak residual response at 1550 nm. The residual below bandgap response of the SiPM was not understood and could be the topic of a complementary study. In any case, we present below a bare polyimide fiber solution that effectively eliminates the light leakage and the related interference with the SiPM's photoresponse.

The "polyimide fiber" (green curve) is a bare polyimide fiber (no tubing jacket) from Thorlabs' FG400LEP multi-mode fiber with a 400 µm core and an NA ~0.22 [48]. Compared to the SiPM current in the dark (black curve: "No light"), obtained in complete darkness, the polyimide fiber exhibited no measurable light leakage over the temperature range studied here.

Given its promising attributes, the bare polyimide fiber has been further tested for cryogenic applications. A 10 m fiber patchcord of the bare polyimide fiber was used, fully immersed into liquid nitrogen. The patchcord had FC connectors on both ends, with its input end connected to a 1466 nm laser source (kept at ~20 °C). Its output end was connected to an AFBR-POC205A8 LPC device, also immersed in liquid nitrogen. Figure 6 shows the measured electrical output of the LPC at 77 K for different optical input powers. Therefore, the 1466 nm light was transmitted through 10 m of bare polyimide multi-mode fiber immersed at 77 K. An electrical output of P_{mpp} = 1.97 W was obtained for an optical input power of 3.0 W. These results demonstrate a conversion efficiency of Eff = 65.7% after 10 m transmission within liquid nitrogen, with an output voltage of V_{mpp} = 6.85 V and an optimal load of R_{mpp} = 23.8 ohms. It should be noted that the measured performance therefore included both the photovoltaic efficiency and the transmission efficiency. The device performance was found to be very similar if the 10 m fiber length was immersed at 77 K compared to the case if only the LPC was immersed, with most of the fiber length kept at room temperature. For example, with a room-temperature optical transmitted power of 1.042 ± 0.005 W, the bare polyimide fiber retained a transmitted power of 1.036 ± 0.005 W once immersed at 77 K in liquid nitrogen. In stark contrast, performing the equivalent test with a common fiber with a furcation tubing jacket, we measured an optical transmitted power of 1.006 W with the fiber at room temperature, but only 0.4 W once immersed at 77 K in liquid nitrogen. The latter observation further confirms that the bare polyimide fiber substantially transmitted all the light even at cryogenic temperatures.

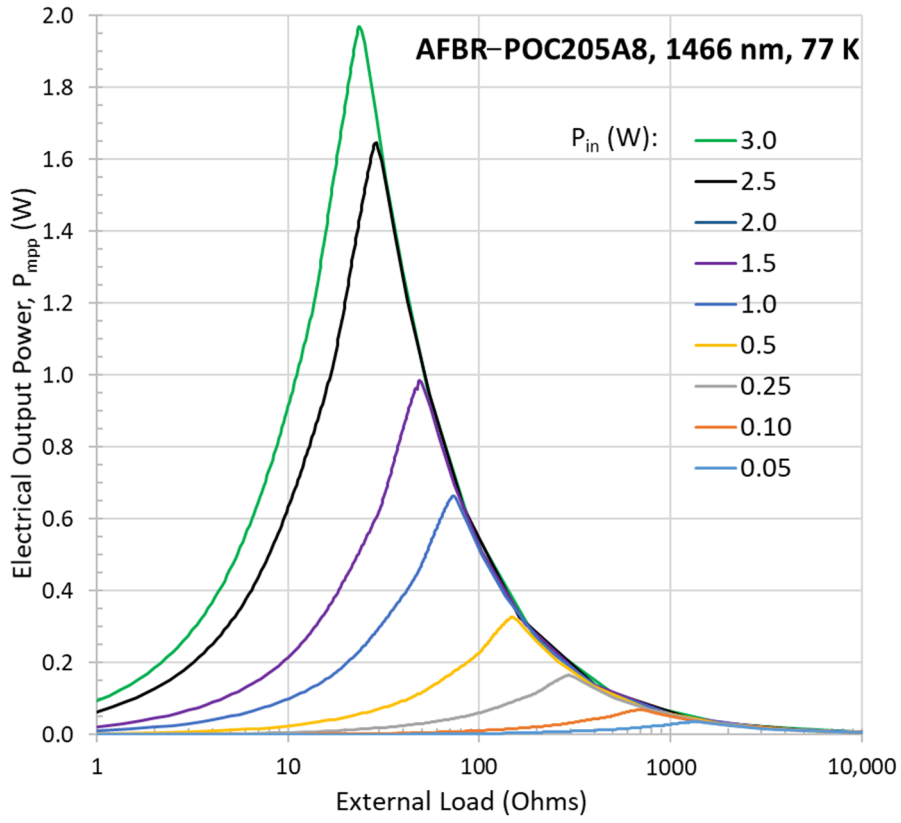

Figure 6. Measured electrical output at 77 K for different optical input powers at 1466 nm transmitted through 10 m of bare polyimide multi-mode fiber, converted using Broadcom's AFBR-POC205A8 multijunction PT10-InGaAs/InP laser power converter.

4. Discussion

We verified that the transmission losses measured with the commercial single-mode and multi-mode fibers are consistent with the values typically specified from the manufacturers. With more powerful 1550 nm sources and using single-mode fibers, Ma et al. demonstrated ~3.5 W of transmitted optical power for a 5 km link, ~1.5 W of transmitted optical power for a 10 km link, and ~0.5 W of transmitted optical power for a 20 km link [1]. Extrapolating our single-mode results in Figure 2 to those that demonstrated higher transmitted optical powers from Ma et al., the AFBR-POC205A9 LPC capabilities are expected to reach an electrical output of $P_{mpp} > 1.6$ W, $P_{mpp} > 0.7$ W, and $P_{mpp} > 0.23$ W for the 5 km, 10 km, and 20 km links, respectively. These high-electrical-output power capabilities are possible with the AFBR-POC205A9 LPCs because of the higher output voltage of the multijunction design and because of their high conversion efficiencies (Eff > 47% at 1550 nm from Figure 2). The multi-mode results in Figure 3 further validate the high conversion efficiency and high output power capabilities of Broadcom's AFBR-POC205Ax LPCs. The conversion efficiency was maintained at least up to 1 W of electrical output power with no measurable performance saturation.

Figures 4 and 5 reveal that certain fiber configurations can be susceptible to light leakage along the fiber length. The most probable origin of the observed light leakage is expected to be related to the microscopic variations in the glass guiding. Jacketed fibers seemed particularly prone to light leakage at low temperatures, for which case, the light leakage was observed to become increasingly more pronounced.

The results are consistent with compression effects from the jacket, which are believed to be responsible for the additional light leakage at low temperatures. We observed that compression effects in the optical connector/ferrule areas can also induce light leakage and transmission losses at lower temperatures.

For example, this was observed in experiments using the LPC as a control device, using different fiber types. We measured the light delivered to a given LPC device down to a temperature of −50 °C from a bare polyimide fiber and compared directly with the results obtained with a "common fiber". An example of such results is shown in Figure 7 for AFBR-POC205A9 LPCs measured at about 1470 nm. Similar to Figure 4 or Figure 5, significant transmission losses could be observed when fiber types other than the bare polyimide fiber were used.

The low-temperature transmission losses were also observed to vary significantly within a group of fibers from nominally the same type. The fiber light leakage losses for the example in Figure 7 was evaluated to about 7% at −40 °C. Overall, the light leakage losses at −50 °C, for a pigtail length of the order of 1 m, were observed to vary from ~0 dB to greater than 3 dB for the various pigtails we examined.

It should be noted that our study should not be extrapolated to infer that light leakage from jacketed fibers at room temperature occurs for all wavelengths or generally across many SM or MM fiber types. Surely, fibers exhibiting low transmission losses (e.g., as in Figure 1) must have very little light leakage. However, for the 808 nm cases examined or for the 1500 nm low-temperature case, it was possible to use the SiPM to help to locally resolve the origin of the light leakage. Some of the fiber pigtails displayed light leakage near the fiber connector area, with little or no light leakage along the fiber pigtail. Other pigtails displayed the opposite effect, with no or little light leakage near the connector area but some light leakage along the fiber length.

The light-sensitive SiPM can be shielded in low-temperature applications by covering the fiber with a loose tube jacket opaque to the transmitted light to block any residual light leakage. However, precautions must be taken to avoid additional jacket compressions on the fiber, which could actually further promote light leakage. In any case, our study revealed that large-core bare polyimide multi-mode fibers can be successfully used to transmit nearly 100% of the incident light through tens of meters of fiber immersed in liquid nitrogen.

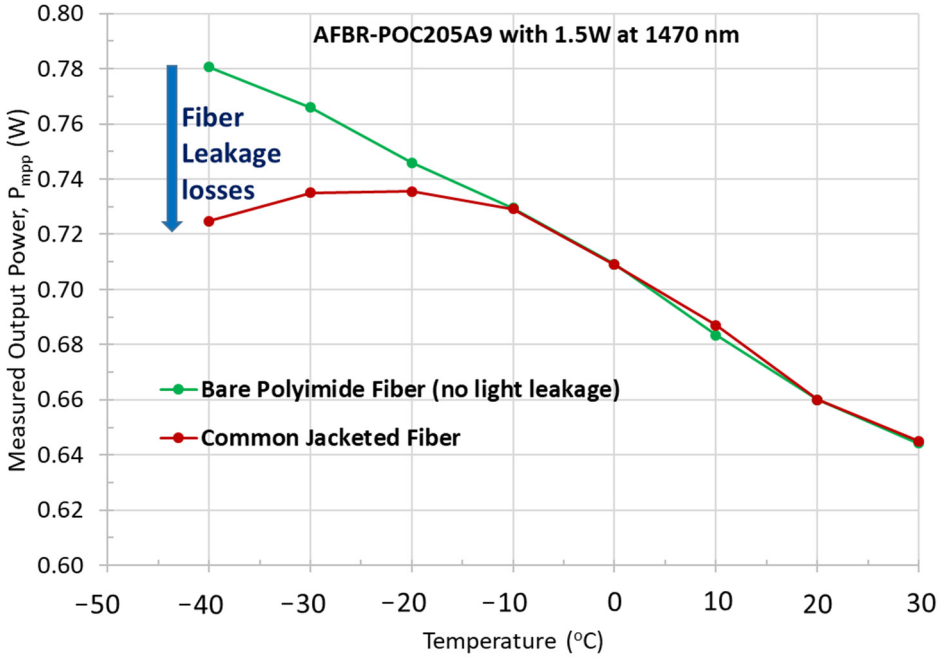

Figure 7. Measured output power as a function of temperature for an AFBR-POC205A9 LPC with 1.5 W of optical input at about 1470 nm. Fiber light leakage can parasitically reduce the measured LPC output power at lower temperatures when fiber types other than bare polyimide fibers are used.

5. Conclusions

In this study, long-distance, high-efficiency power-over-fiber has been demonstrated using ~5 V multijunction photovoltaic power converters. Fiber light leakage effects have been studied for different fiber configurations, and detailed measurements have been made using highly light-sensitive silicon photomultiplier (SiPM) photodetectors. We examined the transmission through single-mode and multi-mode fibers at the wavelengths of 808 nm and 1470/1550 nm. Watts of electrical power for long-distance or cryogenic applications have been delivered with the full galvanic isolation of power-over-fiber.

An electrical output power of ~0.1 W was converted with an LPC conversion efficiency of Eff > 47% after 5 km of transmission through a standard single-mode SMF28 fiber fed with 0.25 W of optical power. It is expected that higher output powers and/or longer distances can readily be achieved by using more powerful optical input sources at 1550 nm [1]. Multi-mode fiber transmission also gave access to high PoF output powers at long distances. An electrical output power of ~1 W was demonstrated with an LPC conversion efficiency of Eff ~49% after 5 km of transmission with a standard OM1 multi-mode fiber fed with ~2.5 W of optical input power at ~1470 nm.

A cryogenic power-over-fiber system at ~1470 nm was also demonstrated with ~2 W of electrical power converted over a 10 m distance, with a conversion efficiency of Eff > 65% at 77 K. Our study demonstrates that specific fiber types can enable low-loss transmission, compatible with cryogenic requirements, and with minimal light leakage triggering of the SiPM.

Author Contributions: Conceptualization, S.F. and D.M; methodology, S.F. and D.M.; software, S.F. and D.M.; validation, S.F. and D.M.; formal analysis, S.F. and D.M.; investigation, S.F. and D.M.; data curation, S.F. and D.M.; writing—original draft preparation S.F.; writing—review and editing S.F. and D.M.; visualization, S.F.; project administration, S.F. and D.M.; funding acquisition, S.F. and D.M. All authors have read and agreed to the published version of the manuscript.

Funding: This research received no external funding.

Institutional Review Board Statement: Not applicable.

Informed Consent Statement: Not applicable.

Data Availability Statement: The data that support the findings of this study are available from the corresponding author upon reasonable request.

Acknowledgments: The authors would like to thank William A. Pellico and his group at Fermilabs for numerous fruitful discussions and support on the cryogenic applications.

Conflicts of Interest: The authors declare no particular conflicts of interest, but it should be noted that the authors are employed by Broadcom, a company that manufactures and sells semiconductor components, including power converter devices.

References

1. Ma, L.; Tsujikawa, K.; Hanzawa, N.; Yamamoto, F. Design of optical power delivery network based on power limitation of standard single-mode fiber at a wavelength of 1550 nm. *Appl. Opt.* **2015**, *54*, 3720–3724. [CrossRef]
2. Peña, R.; Algora, C.; Matías, I.R.; López-Amo, M. Fiber-based 205-mW (27% efficiency) power-delivery system for an all-fiber network with optoelectronic sensor units. *Appl. Opt.* **1999**, *38*, 2463–2466. [CrossRef] [PubMed]
3. Hu, X.; Chen, W.; Chen, M.; Meng, Z. Experimental observation of the competition between stimulated Brillouin scattering, modulation instability and stimulated Raman scattering in long single mode fiber. *J. Opt.* **2016**, *18*, 085501. [CrossRef]
4. Werthen, J.-G. Powering Next Generation Networks by Laser Light over Fiber. In *Optical Fiber Communication Conference*; OWO3; Optica Publishing Group: Washington, DC, USA, 2008.
5. Nugent, T.J. Remote Electric Power Delivery via High Power Laser. In *Applied Industrial Optics 2019, OSA Technical Digest*; Optica Publishing Group: Washington, DC, USA, 2019; paper T3A.4.
6. Bottger, G.; Dreschmann, M.; Klamouris, C.; Hubner, M.; Roger, M.; Bett, A.W.; Kueng, T.; Becker, J.; Freude, W.; Leuthold, J. An optically powered video camera link. *IEEE Photonics Technol. Lett.* **2007**, *20*, 39–41. [CrossRef]
7. Cardona JD, L.; Lallana, P.C.; Altuna, R.; Fresno-Hernández, A.; Barreiro, X.; Vázquez, C. Optically feeding 1.75 W with 100 m MMF in efficient C-RAN front-hauls with sleep modes. *J. Light. Technol.* **2021**, *39*, 7948–7955. [CrossRef]
8. Helmers, H.; Armbruster, C.; von Ravenstein, M.; Derix, D.; Schöner, C. 6-W optical power link with integrated optical data transmission. *IEEE Trans. Power Electron.* **2020**, *35*, 7904–7909. [CrossRef]
9. Fakidis, J.; Helmers, H.; Haas, H. Simultaneous wireless data and power transfer for a 1-Gb/s GaAs VCSEL and photovoltaic link. *IEEE Photonics Technol. Lett.* **2020**, *32*, 1277–1280. [CrossRef]
10. Soref, R.; De Leonardis, F.; Daligou, G.; Moutanabbir, O. Directed high-energy infrared laser beams for photovoltaic generation of electric power at remote locations. *APL Energy* **2024**, *2*, 026101. [CrossRef]
11. Miyamoto, T. Optical WPT. In *Theory and Technology of Wireless Power Transfer*; CRC Press: Boca Raton, FL, USA, 2024; pp. 179–245.
12. Aveta, F.; Basnet, S. Experimental Demonstration of Power over Fiber for Optical Communication System. In *Optical Fibers and Sensors for Medical Diagnostics, Treatment, and Environmental Applications XXIV*; SPIE: Cergy, France, 2024; Volume 12835, pp. 115–122.
13. Garkushin, A.A.; Krishtop, V.V.; Storozhev, S.A.; Volkhin, I.L.; Nifontova, E.V.; Urbanovich, E.V.; Kustov, D.A.; Kadochikov, I.V. Digital Twin of the Photoelectric Converter of the Power Transmission System over Optical Fiber. *J. Phys. Conf. Ser.* **2024**, *2701*, 012146. [CrossRef]
14. Zheng, Y.; Zhang, G.; Huan, Z.; Zhang, Y.; Yuan, G.; Li, Q.; Ding, G.; Lv, Z.; Ni, W.; Shao, Y.; et al. Wireless laser power transmission: Recent progress and future challenges. *Space Sol. Power Wirel. Transm.* 2024, *in press*. [CrossRef]
15. Jaffe, P.; Nugent, T.; Strassner, B., II; Szazynski, M. Power Beaming. In *History, Theory, and Practice*; World Scientific Series on Emerging Technologies: London, UK, 2024; Volume 5, p. 420.
16. Martinek, P.; Prajzler, V. Power over fiber using a large core fiber and laser operating at 976 nm with 10 W power. *Opt. Fiber Technol.* **2023**, *80*, 103404. [CrossRef]
17. Ahnood, A.; Ndabakuranye, J.P.; Li, S.; Kavehei, O.; Prawer, S. Miniature power and data transceiver based on multimodal operation of a single photovoltaic device. *Eng. Res. Express* **2020**, *2*, 015036. [CrossRef]
18. Zhou, Y.; Guan, C.; Lv, H.; Zhang, Y.; Zhou, R.; Chu, W.; Lv, P.; Qin, H.; Li, S.; Li, X. Design and Research of Laser Power Converter (LPC) for Passive Optical Fiber Audio Transmission System Terminal. *Photonics* **2023**, *10*, 1257. [CrossRef]
19. Mukherjee, J.; Jarvis, S.; Perren, M.; Sweeney, S.J. Efficiency limits of laser power converters for optical power transfer applications. *J. Phys. D Appl. Phys.* **2013**, *46*, 264006. [CrossRef]
20. Geisz, J.F.; Friedman, D.J.; Steiner, M.A.; France, R.M.; Song, T. Operando Temperature Measurements of Photovoltaic Laser Power Converter Devices Under Continuous High-Intensity Illumination. *IEEE J. Photovolt.* **2023**, *13*, 808. [CrossRef]
21. Albert, P.; Jaouad, A.; Hamon, G.; Volatier, M.; Valdivia, C.E.; Deshayes, Y.; Hinzer, K.; Béchou, L.; Aimez, V.; Darnon, M. Miniaturization of InGaP/InGaAs/Ge solar cells for micro-concentrator photovoltaics. *Prog. Photovolt. Res. Appl.* **2021**, *29*, 990–999. [CrossRef]
22. Fafard, S.; York, M.C.A.; Proulx, F.; Valdivia, C.E.; Wilkins, M.M.; Arès, R.; Aimez, V.; Hinzer, K.; Masson, D.P. Ultrahigh efficiencies in vertical epitaxial heterostructure architectures. *Appl. Phys. Lett.* **2016**, *108*, 071101. [CrossRef]
23. Matsuura, M. Recent advancement in power-over-fiber technologies. *Photonics* **2021**, *8*, 335. [CrossRef]

24. Acerbi, F.; Paternoster, G.; Merzi, S.; Zorzi, N.; Gola, A. Nuv and vuv sensitive silicon photomultipliers technologies optimized for operation at cryogenic temperatures. *Nucl. Instrum. Methods Phys. Res. Sect. A Accel. Spectrometers Detect. Assoc. Equip.* **2023**, *1046*, 167683. [CrossRef]
25. Delgado, M.; Gutiérrez, R.M.; Fuentes, F. Liquid argon photodetection systems for neutrino detectors: A minireview. *J. Phys. Conf. Ser.* **2020**, *1672*, 012009. [CrossRef]
26. Brizzolari, C.; Carniti, P.; Cattadori, C.; Cristaldo, E.; de la Torre Rojo, A.; Delgado, M.; Falcone, A.; Francis, K.; Gallice, N.; Gotti, C.; et al. Cryogenic front-end amplifier design for large SiPM arrays in the DUNE FD1-HD photon detection system. *J. Instrum.* **2022**, *17*, P11017. [CrossRef]
27. Temples, D.J.; McLaughlin, J.; Bargemann, J.; Baxter, D.; Cottle, A.; Dahl, C.E.; Lippincott, W.H.; Monte, A.; Phelan, J. Measurement of charge and light yields for Xe 127 L-shell electron captures in liquid xenon. *Phys. Rev. D* **2021**, *104*, 112001. [CrossRef]
28. Abud, A.A.; Abi, B.; Acciarri, R.; Acero, M.A.; Adames, M.R.; Adamov, G.; Adamowski, M.; Adams, D.; Adinolfi, M.; Aduszkiewicz, A.; et al. Scintillation light detection in the 6-m drift-length ProtoDUNE Dual Phase liquid argon TPC. *Eur. Phys. J. C* **2022**, *82*, 618. [CrossRef] [PubMed]
29. Ezzouine, Z.; Danovitch, D.; Bechou, L.; Pioro-Ladrière, M.; Lacerte, M. Contact resistance behavior of land grid array sockets at cryogenic temperatures required for quantum measurements. *IEEE Trans. Compon. Packag. Manuf. Technol.* **2021**, *11*, 367. [CrossRef]
30. Lindholm, E.A.; Stolov, A.A.; Dyer, R.S.; Slyman, B.; Burgess, D. Reliability of Optical Fibers in a Cryogenic Environment. In Proceedings of the Fiber Optic Sensors and Applications VI, Orlando, FL, USA, 13–17 April 2009; SPIE: Bellingham, WA, USA, 2009; Volume 7316, pp. 258–263.
31. Fafard, S.; Masson, D.P. Perspective on photovoltaic optical power converters. *J. Appl. Phys.* **2021**, *130*, 160901. [CrossRef]
32. Fafard, S.; Masson, D.P. High-Efficiency and High-Power Multijunction InGaAs/InP Photovoltaic Laser Power Converters for 1470 nm. *Photonics* **2022**, *9*, 438. [CrossRef]
33. Fafard, S.; Masson, D.P. 74.7% Efficient GaAs-Based Laser Power Converters at 808 nm at 150 K. *Photonics* **2022**, *9*, 579. [CrossRef]
34. Fafard, S.; Masson, D. 67.5% Efficient InP-Based Laser Power Converters at 1470 nm at 77 K. *Photonics* **2024**, *11*, 130. [CrossRef]
35. Helmers, H.; Lopez, E.; Höhn, O.; Lackner, D.; Schön, J.; Schauerte, M.; Schachtner, M.; Dimroth, F.; Bett, A.W. 68.9% Efficient GaAs-Based Photonic Power Conversion Enabled by Photon Recycling and Optical Resonance. *Phys. Status Solidi (RRL) Rapid Res. Lett.* **2021**, *15*, 2100113. [CrossRef]
36. Algora, C.; García, I.; Delgado, M.; Peña, R.; Vázquez, C.; Hinojosa, M.; Rey-Stolle, I. Beaming power: Photovoltaic laser power converters for power-by-light. *Joule* **2022**, *6*, 340–368. [CrossRef]
37. Wang, A.-C.; Yin, J.-J.; Yu, S.-Z.; Sun, Y.-R.; Dong, J.-R. Origins of the short circuit current of a current mismatched multijunction photovoltaic cell considering subcell reverse breakdown. *Opt. Express* **2023**, *31*, 14482–14494. [CrossRef] [PubMed]
38. Beattie, M.N.; Valdivia, C.E.; Wilkins, M.M.; Zamiri, M.; Kaller, K.L.C.; Tam, M.C.; Kim, H.S.; Krich, J.J.; Wasilewski, Z.R.; Hinzer, K. High current density tunnel diodes for multi-junction photovoltaic devices on InP substrates. *Appl. Phys. Lett.* **2021**, *118*, 062101. [CrossRef]
39. Khvostikov, V.P.; Sorokina, S.V.; Khvostikova, O.A.; Nakhimovich, M.V.; Shvarts, Z. Ge-Based Photovoltaic Laser-Power Converters. *IEEE J. Photovolt.* **2023**, *13*, 254–259. [CrossRef]
40. Kalyuzhnyy, N.A.; Malevskaya, A.V.; Mintairov, S.A.; Mintairov, M.A.; Nakhimovich, M.V.; Salii, R.A.; Shvarts, M.Z.; Andreev, V.M. Photovoltaic AlGaAs/GaAs devices for conversion of high-power density laser (800–860 nm) radiation. *Sol. Energy Mater. Sol. Cells* **2023**, *262*, 112551. [CrossRef]
41. Gou, Y.; Zhu, L.; Mou, Z.; Chen, Y.; Cheng, Y.; Wang, J.; Yang, H.; Deng, G. InP-based tunnel junctions for ultra-high concentration photovoltaics. *Opt. Express* **2024**, *32*, 408–414. [CrossRef] [PubMed]
42. Helmers, H.; Oliva, E.; Schachtner, M.; Mikolasch, G.; Ruiz-Preciado, L.A.; Franke, A.; Bartsch, J. Overcoming Optical-Electrical Grid Design Trade-Offs for cm2-Sized High-Power GaAs Photonic Power Converters by Plating Technology. *Prog. Photovolt. Res. Appl.* 2024, *in press*. [CrossRef]
43. Gou, Y.; Mou, Z.; Wang, H.; Chen, Y.; Wang, J.; Yang, H.; Deng, G. High-performance laser power converters with resistance to thermal annealing. *Opt. Express* **2024**, *32*, 8335–8342. [CrossRef] [PubMed]
44. Optical Fibers from Fiber Instrument Sales (FIS) Were Used in This Study for the 1-km and 5-km Single-Mode and Multi-Mode Fiber Cables. The Single-Mode Fiber is a Corning SMF28-Ultra with a Core Diameter of 8.2 μm, Cladding of 125 μm, and NA ~0.14. The Multi-Mode Fiber is a Standard Graded-Index Corning InfiniCor OM1 Fiber with a Core Diameter of 62.5 μm, Cladding of 125 μm, and NA ~ 0.275. Available online: https://www.fiberinstrumentsales.com/ (accessed on 3 June 2024).
45. BWT Beijing Ltd. Laser Diodes were Used as Multi-Mode Sources: A 7W ~1470 nm Source with a 105 μm Core was Used for the MM Experiements at 20 °C and a 8W~808 nm Source with a 400 μm Core was Used for the MM Experiements at 77 K. Available online: https://www.bwt-bj.com/en/product/ (accessed on 3 June 2024).
46. A SemiNex Corporation Laser Diode was Used as a High-Power Single-Mode 1550 nm Source with a 10 nm Spectral-Width. Available online: https://seminex.com/ (accessed on 3 June 2024).
47. A Lens-Coupler from OzOptics Limited was Used in this Study to Couple the 105 μm Core Fiber Laser Source to the Standard 62.5 μm Core OM1 Fiber: Part #AA-300-33-1550-M-SP1. Available online: https://www.ozoptics.com/ (accessed on 3 June 2024).

48. Optical Fibers from Thorlabs Were Used in This Study for the Bare Polyimide Fibers. Available online: https://www.thorlabs.com/ (accessed on 3 June 2024).
49. Laser Power Converters from Broadcom Were Used in This Study. Available online: https://www.broadcom.com/products/fiber-optic-modules-components/industrial/optical-power-components/optical-power-converters/ (accessed on 3 June 2024).